

Suppression of Transition Behind a Discrete Roughness Element Using a Downstream Element

Alexandre R. Berger, Madeline N. McMillan, Edward B. White

Department of Aerospace Engineering
Texas A&M University
College Station, Texas 77840
alex.rj.berger@gmail.com, mad_mcmillan@tamu.edu, ebw@tamu.edu

Saikishan Suryanarayanan, David B. Goldstein

Department of Aerospace Engineering and Engineering Mechanics
The University of Texas at Austin
Austin, Texas 78712
saikishan.suryanarayanan@gmail.com, david@ices.utexas.edu

ABSTRACT

Discrete roughness elements in laminar boundary layers trigger breakdown to turbulence when the associated roughness Reynolds number, Re_{kk} , exceeds a critical value. Recent work by Suryanarayanan et al. (2017a) has demonstrated that for the case of a 45°-inclined rectangular roughness at modest supercritical Re_{kk} , transition can be prevented by placing a second oppositely inclined rectangular roughness element in the wake of the upstream element. Extensive hotwire measurements downstream of the single and two-element roughness configurations are made to determine how the addition of the second element suppresses transition. The data show that although the second element does not dramatically reduce the maximum velocity disturbance, disturbance velocity gradients are reduced and, as a result, unsteady velocity fluctuations do not grow as quickly. Then, as the wake recovers, the unsteady fluctuations decay without forming a turbulent wedge. Two-dimensional eigenmode calculations are made using measured steady flow data and these corroborate the measured fluctuation data.

INTRODUCTION

Maintaining laminar flow in boundary layers provides better aerodynamic efficiency than turbulent flow by virtue of the lower wall shear stress of a laminar boundary layer. In practice, maintaining laminar flow at the Reynolds numbers of operating aircraft is extremely difficult. High Re values produce strong instability growth that leads to turbulence and thin boundary layers enable even small surface imperfections to generate significant boundary-layer disturbances.

In the context of suppressing or delaying laminar-to-turbulent transition in 2D (i.e., unswept) boundary layers, the focus of this paper is investigation of a transition mitigation strategy proposed by Sharma et al. (2014) and Sharma and Goldstein (unpublished) that was later demonstrated by Suryanarayanan et al. (2017a). The approach eliminates a turbulent wedge generated by a modestly supercritical discrete roughness element (DRE) consisting of a 45°-inclined rectangle. Using direct numerical simulation (DNS) Sharma and Goldstein found that placing a second, somewhat smaller element in the wake of the first with opposite inclination eliminates the turbulent wedge.

The historical literature has extensive work regarding the role of discrete roughness elements and their effect on transition in low-speed, 2D boundary layers. Since the 1950s, transition in

the wake of isolated three-dimensional roughness elements has been effectively predicted using correlations based on a roughness-based Reynolds number $Re_{kk} = U(k)k/\nu$ (see, e.g., Tani 1969 and von Doenhoff and Braslow 1961). If Re_{kk} of a roughness element exceeds $Re_{kk,crit}$, then transition is expected to occur at or just aft of the roughness element. If the critical value is not exceeded, no effect is expected. $Re_{kk,crit}$ is expected to be between 600 and 900 for a roughness element with approximately equal height, k , and diameter, d . For other shapes, von Doenhoff and Braslow suggest that $Re_{kk,crit}$ varies as $(k/d)^{2/5}$. Thus, many recent studies with low values of k/d transition at Re_{kk} values at or below 300.

The mechanism by which the DREs lead to transition was investigated by Ergin and White (2006) in an experiment similar to that performed here. Ergin and White used circular DREs with $Re_{kk,crit} \leq 334$ and found that the mechanism that brought about breakdown to turbulence exists in the $\partial U/\partial y$ and $\partial U/\partial z$ shear layers above low-speed streaks in DRE wakes.

The recent work by Suryanarayanan et al. (2017a) demonstrates that the mechanism proposed by Sharma and Goldstein is effective and is somewhat robust to geometry variations of the downstream element. Figure 1 is a composite of naphthalene flow-visualization images with and without a control DRE. The images clearly show that the addition of the control DRE eliminates the turbulent wedge visible in the bottom image and leaves only a long-lived high-shear streak in the wake of the pair of elements.

While Suryanarayanan et al. (2017a) demonstrated that the second element is effective, that study did not reveal how transition suppression is achieved. The present paper seeks to illuminate the underlying suppression mechanism. The work consists of extensive experimental measurements in the wake of a single 45°-inclined DRE that produces a turbulent wedge and a pair of oppositely inclined elements that do not. Mean and fluctuating velocities downstream of both configurations are measured and analyzed to show how unstable fluctuations grow in the wake of the single-element configuration while similar fluctuations do not grow in the double-element case. Additionally, the experimentally measured mean flows are used as input to a 2D eigenvalue solver and resulting mode shapes and growth rates are estimated using a linear-stability code.

It is important to note that this investigation is limited to just features that can be measured in the wake of the roughness element (or elements). The underlying assumption is that because breakdown to turbulence occurs after some incubation distance down-



Figure 1. Naphthalene flow-visualization images. The top image shows how a second downstream DRE eliminates the turbulent wedge that occurs in the bottom single-DRE image. Figure adapted from Suryanarayanan et al. (2017a).

stream of the roughness, an instability process causes disturbances to grow to sufficient amplitude to cause transition. While much can be learned using this approach, we are unable to investigate the near-field details of the flow over the roughness elements. Thus, the way in which the roughness shapes produce the wakes is not a question this paper can answer. A suitable near-field analysis is the domain of DNS or another experimental technique.

To this end, a companion paper by Suryanarayanan et al. (2017b) studies the same problem using DNS and examines the suppression phenomenon from a vorticity dynamics viewpoint. There is close collaboration between the experimental work reported here and the accompanying DNS. Good agreement is achieved between the two approaches. Details of the simulation are reported by Suryanarayanan et al. (2017b).

APPROACH

Similar to the work reported earlier by Suryanarayanan et al. (2017a), the roughness studied here consists of rectangular discrete roughness elements (DREs) situated on a flat plate that provides a Blasius boundary layer. Adjustable mounting brackets allow the plate to be aligned for near zero-pressure gradient. The basis for these adjustments are measurements boundary-layer profiles without roughness present. The plate inclination is adjusted until the shape factor is $H = 2.59 \pm 0.04$.

Two main roughness configurations are studied. First is a single element inclined 45° to the flow direction with side lengths $l_1 = 12.6$ mm and $b_1 = 4.57$ mm. (See Fig. 2 for the definitions of various dimensions.) The element is 1.27 mm thick. The element is manufactured from aluminum and is cut with multiple facets that match the DNS grid. The element is located 1385 mm downstream of the physical leading edge of the flat plate where the boundary-layer displacement thickness is $\delta^* = 2.44$ mm.¹

The second roughness configuration adds a second “control” roughness element downstream of the first. The control DRE is located $\lambda = 7.23$ mm downstream and is offset by $c = 3.6$ mm in the spanwise direction. It is inclined -45° to the flow, opposite the first element. Following Suryanarayanan et al. (2017a), this second element is only 83% the thickness of the upstream element, 1.05 mm thick. Its side dimensions are $\lambda_2 = 9.56$ mm and $b_2 = 4.57$ mm.

During experiments the wind tunnel is maintained at a con-

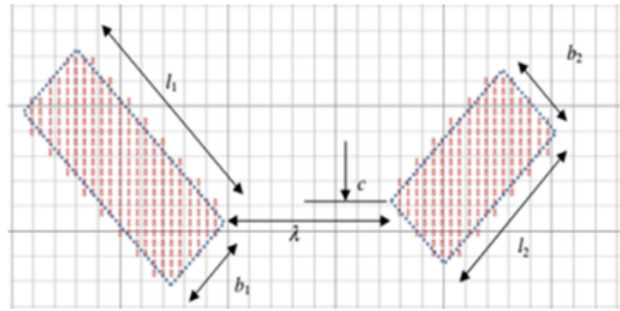


Figure 2. DRE geometry definition. Flow is from left to right.

stant unit Reynolds number, $Re' = U_\infty/\nu = 600\,000/\text{m}$ which corresponds to approximately 11 m/s. At this Re' and roughness location the roughness height corresponds to $Re_{kk} \approx 230$. This is sufficient to trip a turbulent wedge behind a single inclined DRE. When the control element is added, transition does not occur. (See Fig. 1.)

The experiments are performed in the Klebanoff-Saric Wind Tunnel (KSWT) at Texas A&M University. The KSWT is a closed-return, low-disturbance wind tunnel used extensively for experiments on low-speed boundary layer stability and transition. To this end, the KSWT is designed to provide an extremely low freestream turbulence intensity of 0.02%. Facility details are given by Hunt et al. (2010).

Measurements are made using a pair of constant-temperature hotwire anemometers calibrated for velocity and temperature. One wire was moved through the boundary layer in y - z (wall-normal-spanwise) planes at various downstream locations while the other wire made instantaneous freestream velocity measurements. Measurements extended from the freestream, multiple millimeters outside the boundary layer to within several hundred microns of the plate surface where $U/U_{\text{edge}} < 0.1$. Two-second samples were obtained at each point at a 10 kHz sample rate so well-resolved u' spectra could be obtained. Measurements were made at streamwise locations from $x = 1420$ mm, 35 mm downstream of the upstream of the first roughness element to $x = 1600$ mm. Hotwire data is recorded as mean values, U ; rms fluctuations, u'_{rms} and u' spectra.

¹All streamwise coordinates are given relative to the physical leading edge of the flat plate. The virtual origin of Blasius flow is 167 mm downstream of the physical leading edge.

RESULTS

Running at $Re' = 600000/m$ produces velocity contours similar to those shown in Fig. 3. These plots show the the wake of the single DRE (left) and the “control” DRE pair (right), at $x = 1550$ mm, 165 mm downstream of the center of the upstream DRE. Black lines are lines of constant mean velocity (10% levels of U_{edge}) and color contours are u'_{rms} levels. What is notable is that the maximum mean velocity disturbance relative to Blasius flow (at the edges of each figure) is roughly equal with and without the downstream control DRE. That is, the control DRE does not decrease the overall mean velocity disturbance at this station.

In spite of the control DRE not substantially changing the steady velocity disturbance, it does substantially reduce the intensity of u'_{rms} fluctuations compared to the single-DRE case. In the single DRE case, these fluctuations are mostly situated above a decelerated streak centered about $z = 7$ mm on the left plot of Fig. 3 where $\partial U/\partial y$ shear is large. Compared to the two-DRE case, the large-amplitude $\partial U/\partial y$ shear is located farther from the surface with a significant low-speed streak below. This pattern provides favorable conditions for instability growth. The spanwise mean shear $\partial U/\partial z$ is also more pronounced in the single-DRE case and high levels of u'_{rms} are observed wrapping down the sides of the low-speed streak. No significant velocity fluctuations are observed at negative z values to the left of the high-speed streak that is located near $z = 0$.

The DNS results obtained by Suryanarayanan et al. (2017b) are in qualitative agreement with the experimental measurements. Figure 4 shows DNS results 35 mm downstream of a single DRE. The simulation results for u'_{rms} grow somewhat earlier for the experiments so the best match is seen at different x locations for the experiment and DNS. This phenomenon has been seen in earlier work by Suryanarayanan et al. (2017a) and in other collaborative efforts between DNS by Goldstein and co-workers and matched experiments in the KSWT. Notwithstanding the somewhat different downstream location for the two methods, the same general result is observed. The single DRE produces a low-speed streak and high-intensity u'_{rms} fluctuations exist above the streak and grow to form a turbulent wedge. When the second “control” DRE is added, strong U disturbances are produced but these do not lead to transition, apparently because the mean shear is reduced.

To further explore the instability that leads to transition, fluctuation spectra are obtained from the u' time series. Spectra from three locations in the y - z plane are selected in the wake of the single DRE, at $x = 1500$ mm, 115 mm downstream of the roughness. These locations are indicated in Fig. 5 and the corresponding spectra are shown in Fig. 6. The locations correspond to the u'_{rms} peak above the low-speed streak (A), along the flank of the streak (B) and in the undisturbed boundary layer outside the roughness wake. The most-pronounced fluctuations occur between 250 and 300 Hz above the low-speed streak, point (A), and between 45 and 75 Hz along the streak flanks, point (B). Some activity is also observed at higher frequencies which may be a harmonic of the higher-frequency fluctuations at point (A).

All of the hotwire data obtained at all x locations was decomposed into power spectra. Fluctuation power contained in the 250 to 300 Hz ‘A’ band and 45 to 75 Hz ‘B’ band was calculated by integrating the power spectra between those frequency limits at each point in space. Plotting the results yields figures such as those shown in Fig. 7 that isolate the contribution to the u'_{rms} by the ‘A’ and ‘B’ bands.

The passband contour plots are key to understanding the transition suppression mechanism. The top row of plots shows the lower-frequency ‘B’ band between 45 and 75 Hz. These low-frequency fluctuations seem to represent a small degree of spanwise mean-

dering of the low-speed streak. If the streak were to shift in the z direction, the $\partial U/\partial z$ shear would manifest as a u' velocity fluctuation. This appears to occur in both the single- and two-DRE configurations. The fluctuations are stronger in the single-DRE case, presumably because there is stronger spanwise mean shear.

These low-frequency fluctuations are not observed in the DNS. This may be because the DNS inflow does not provide an appropriate upstream condition to trigger this meandering or because resolving such a low-frequency fluctuation would require many flow-through times for adequate statistical convergence. In any case, the low-frequency fluctuations do not appear to be central to the transition of transition suppression mechanism. They are present with and without the control DRE in the experiment and never appear in the DNS.

Alternatively, the high-frequency fluctuations between 250 and 300 Hz do appear to be central to transition and transition mitigation. These fluctuations exist in the $\partial U/\partial y$ shear above the low-speed streak downstream of the single DRE but are eliminated in the wake of the DRE pair. Eliminating these unsteady fluctuations appears to be the key to preventing formation of a turbulent wedge. These fluctuations appear in the same location and have the same character as the Kelvin–Helmholtz-like fluctuations observed by Ergin and White (2006) in a similar experiment that examined unsteady fluctuations behind cylindrical roughness elements. That paper compared fluctuations in subcritical and supercritical Re_{kk} cases and found a key difference between supercritical and subcritical DRE wakes. In the subcritical case, the boundary-layer relaxes toward Blasius and the shear layers stabilize before transition occurs. In the supercritical case the shear is sufficiently strong and fluctuation growth rates sufficiently fast that transition occurs before the flow can stabilize. In this paper, the second roughness element achieves the same purpose as a lower Re_{kk} by disrupting the strength of the mean shear and reducing instability growth rates.

To rigorously clarify the role of shear-layer instability, the experimental results are compared to linear-stability calculations that provide 2D eigenvalues and eigenmode shapes corresponding to the measured $U(y, z)$ mean-flow contours. The calculation is performed using a spatial, viscous parallel-flow instability solver that finds 2D eigenmodes and corresponding spatial eigenvalues using 2D $U(y, z)$ data provided by DNS, experiments or parabolized Navier–Stokes solvers (Monschke and White 2017). The code has been validated against data from an experiment by Kuester and White (2015) conducted in the KSWT under conditions similar to this work.

Linear-stability results are in good agreement with the measured fluctuation bandpass contours. For the single roughness configuration, the fastest-growing modes are a sinuous instability at 51 Hz that is situated on both sides of the primary DRE wake similar to that shown in the top-left plot of Fig. 7 plus a 201-Hz varicose instability that sits above the wake similar to that shown in the bottom-left plot of Fig. 7. The calculated mode shapes for the single DRE configuration are shown in Fig. 8. Substantially lower growth rates of less-well-defined modes are observed in the wake of the DRE pair consisting of the primary and control DRE. The most-amplified modes in that case are at 47 Hz and 122 Hz and have growth rates less than half those in the case without the control DRE. The 122 Hz fluctuations are situated low in the boundary layer and appear to be associated with $\partial U/\partial z$ fluctuations similar to the lower-frequency fluctuations. They do not appear to have any influence on transition.

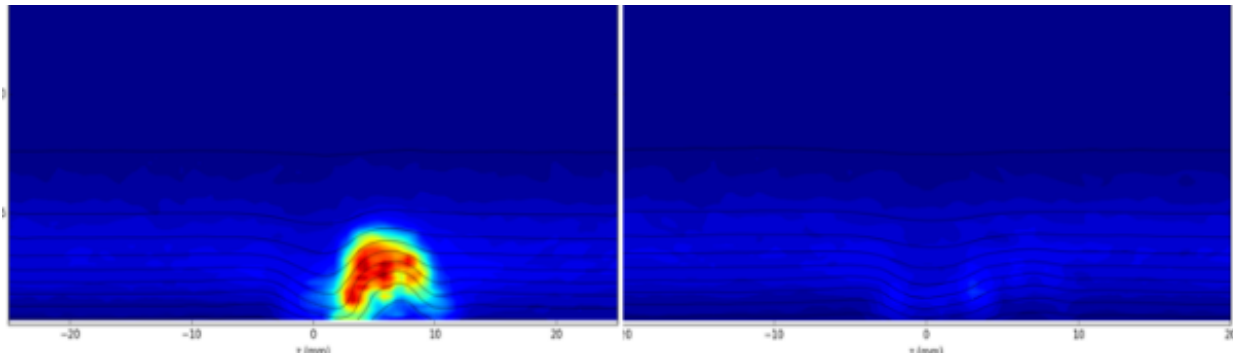


Figure 3. Hotwire measurements of $U(y, z)$ and u'_{rms} (both normalized by U_{edge} at $x = 1550$ mm, 165 mm downstream of the center of the upstream DRE).

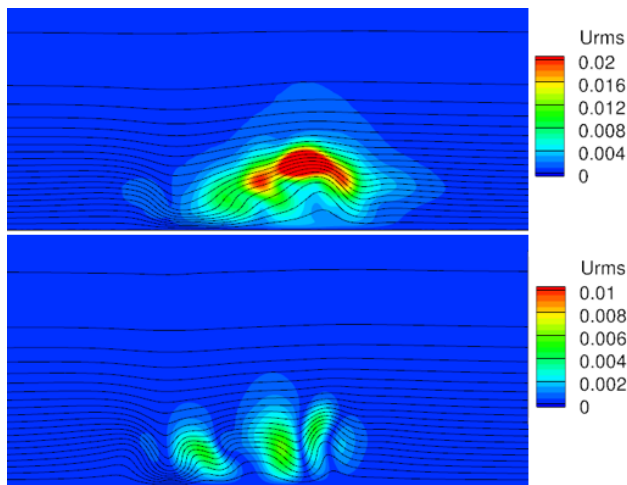


Figure 4. DNS results by Suryanarayanan et al. (2017b) corresponding to experimental U and u'_{rms} contours shown in Fig. 3. The top plot is a single DRE, the lower plot is the “control” DRE pair.

CONCLUSION

Overall, the experiments, DNS and linear-stability results are all in agreement. When only a single 45° -inclined DRE exists at $Re_{kk} \approx 230$, velocity fluctuations centered around 275 Hz grow in the region of strong $\partial U/\partial y$ shear above the low-speed streak in the wake of the roughness element. These fluctuations grow sufficiently large that they lead to breakdown and form a turbulent wedge. All three methods are in agreement about the location and importance of these velocity fluctuations. The experiments and linear-stability analysis are in good agreement about the unstable frequencies.

Lower-frequency fluctuations near 60 Hz are observed along the flanks of the low-speed streak in the experiment and linear-stability results. These are interpreted as spanwise meandering of the streak. These fluctuations are not observed in the DNS either because of the limited simulation duration or because the simulation inflow conditions do not trigger the corresponding fluctuations.

When an oppositely inclined and somewhat smaller DRE is placed in the wake of the first, the experiments and DNS both show that transition is suppressed. The steady velocity disturbance is not significantly reduced in magnitude from the single-DRE case. However, the $\partial U/\partial y$ and $\partial U/\partial z$ mean shear is reduced in strength. This has the effect of substantially reducing instability growth rates. As

a result, the high-frequency fluctuations above the low-speed streak are nearly eliminated and transition does not occur. That is, the transition suppression mechanism appears to be the reduction in strong shear in the roughness wakes due to the introduction of the second element. With weaker shear, high-frequency fluctuations do not grow and transition is suppressed.

ACKNOWLEDGEMENTS

The authors gratefully acknowledge Jason Monschke for his assistance in performing the linear-stability analysis. This work is supported by the U.S. Air Force Office of Scientific Research through grant FA9550-15-1-0345.

REFERENCES

- Ergin, F.G., and White, E.B., 2006, “Unsteady and Transitional Flows Behind Roughness Elements”, *AIAA Journal* **44**:2504–14.
- Hunt, L., Downs, R.S., Kuester, M.S., White, E.B., and Saric, W.S., 2010, “Flow quality measurements in the klebanoff-saric wind tunnel.” AIAA Paper 2010-4538.
- Kuester, M.S., and White, E.B., 2015, “Roughness receptivity and shielding in a flat plate boundary layer.” *J. Fluid Mech.* **777**:430–60.
- Monschke, J.A., and White, E.B., 2017, “BiGlobal Secondary Instabilities of Roughness-Induced Transient Growth,” in preparation.
- Sharma, A., Drews, S. D., Kuester, M. S., Goldstein, D. B., and White, E. B., 2014, “Evolution of Disturbance due to Discrete and Distributed Surface Roughness in Initially Laminar Boundary Layers,” AIAA Paper 2014-0235.
- Suryanarayanan, S., Goldstein, D.B., Brown, G.L., Berger, A.R., and White, E.B., 2017a, “On the Mechanics and Control of Boundary Layer Transition induced by Discrete Roughness Elements,” AIAA Paper 2017-0307.
- Suryanarayanan, S., Goldstein, D.B., Brown, G.L., 2017b, “Roughness Induced Transition In Wall Bounded Flow: A Vorticity Point Of View” Proc. Tenth International Symposium on Turbulence and Shear Flow Phenomena, Chicago.
- von Doenhoff, A. E., and Braslow, A. L., 1961, “The Effect of Distributed Surface Roughness on Laminar Flow,” *Boundary Layer and Flow Control*, edited by G. V. Lachmann, Vol. 2, Pergamon, pp. 657681.
- Tani, I., 1969, Boundary-Layer Transition, *Annual Review of Fluid Mechanics*, **1**:169-96.

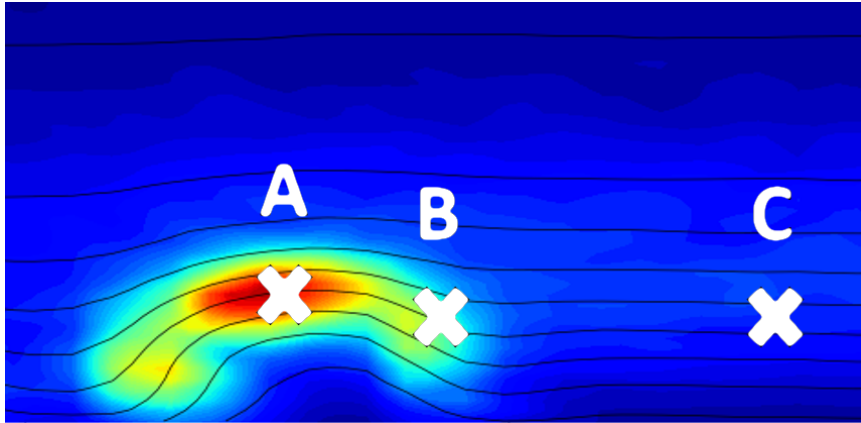


Figure 5. Mean velocity and u'_{rms} contours at $x = 1500$ mm. Labeled points indicate locations at which power spectra in Fig. 6 are obtained.

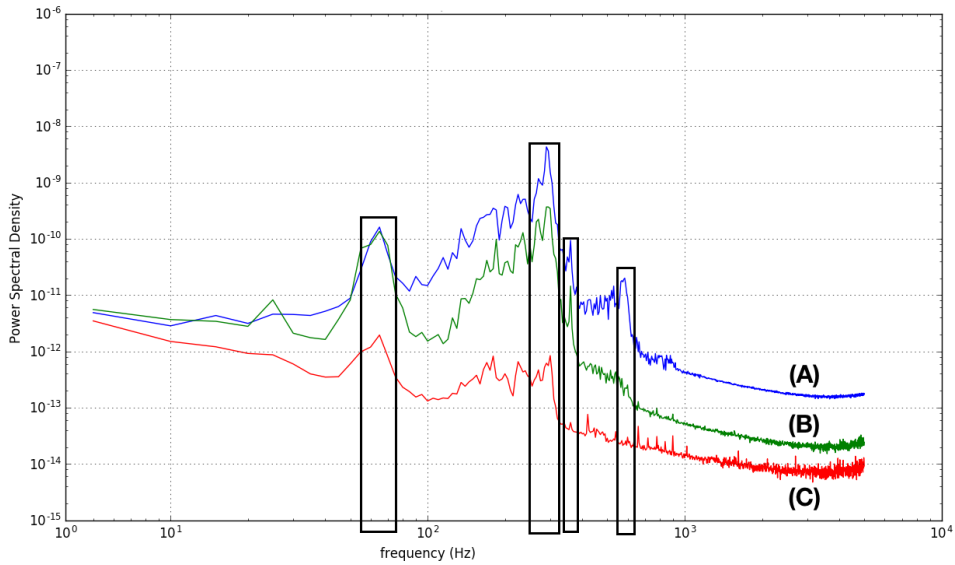


Figure 6. Power-spectra of u' time series measured at locations (A), (B), and (C) in Fig. 5. Boxed frequency bands indicate pass bands for subsequent analysis.

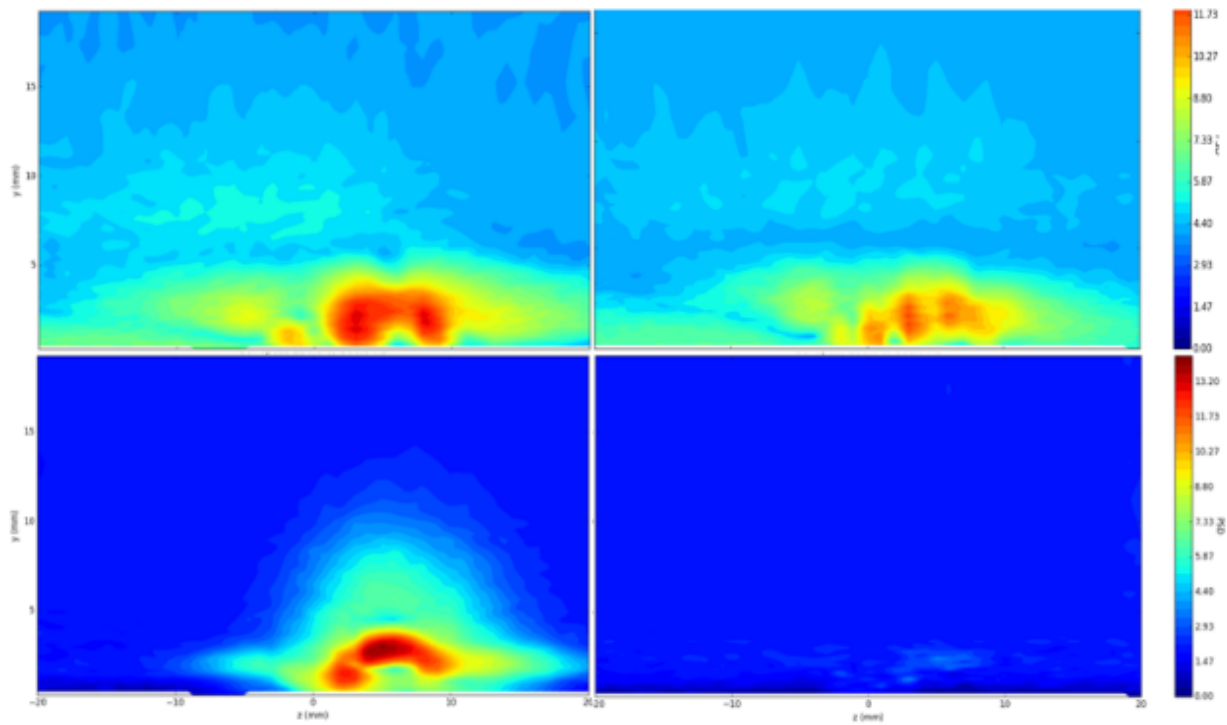


Figure 7. Contours of bandpassed u' fluctuations at $x = 1500$ mm. The left column is the single-DRE case that leads to a turbulent wedge. The right column is the two-element control case that does not. The top row is the 45 to 75 Hz bandpass. The bottom row is the 250 to 300 Hz pass band.

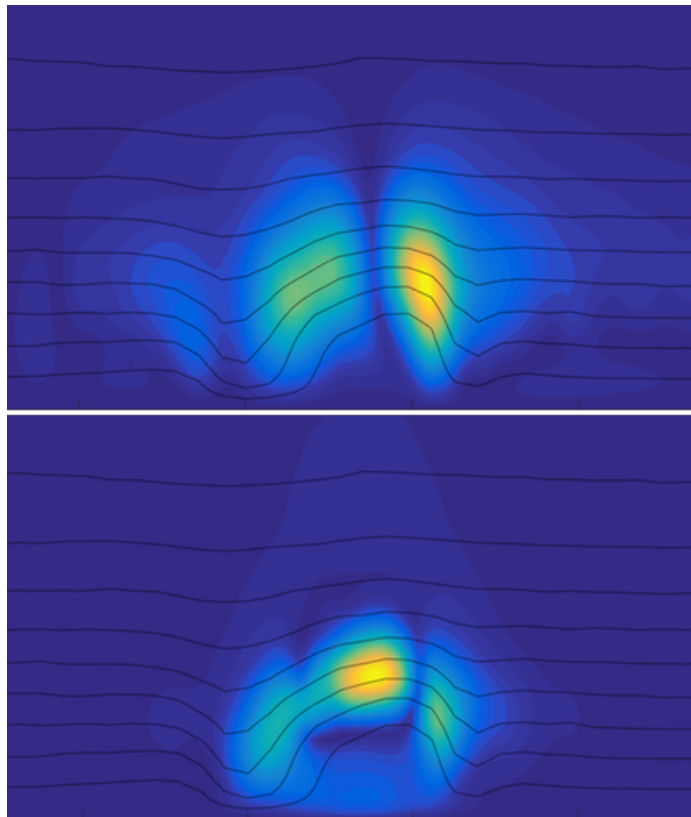


Figure 8. Linear stability mode shapes for $x = 1440$ mm. The top plot is the 47 Hz sinuous mode similar to the top-left plot of Fig. 7. The bottom plot is the 201-Hz varicose mode similar to the bottom-left plot of Fig. 7.